

Computational Analysis of a Boundary Layer Ingesting Tailcone Thruster Configuration Using the LAVA Curvilinear Solver

Luís S. Fernandes **Leonardo G. Machado** **Jeffrey A. Housman**

Computational Aerosciences Branch, NASA Ames Research Center, Moffett Field, California

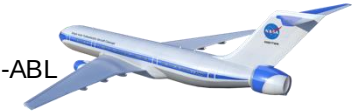
David T. Chan

Configuration Aerodynamics Branch, NASA Langley Research Center, Hampton, Virginia

Advanced Modeling & Simulation (AMS) Seminar Series
NASA Ames Research Center, September 19th, 2024

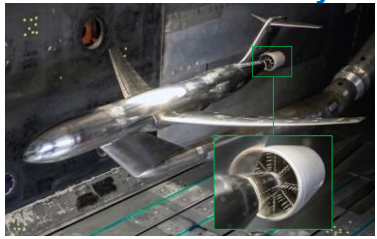
Boundary Layer Ingesting Tailcone System (BLITS)

- **Problem / Objective / Approach**
  - Investigate potential benefit of Type-II BLI systems such as STARC-ABL
    - Ingestion of lower momentum flow ➔ higher propulsive efficiency
    - Propulsion Airframe Integration (PAI) effects may overwhelm or negate benefit
  - Develop integrated airframe-turbomachinery computational simulation capability
    - Enable system-level predictions for tightly-coupled PAI configurations
  - Conduct ground experiments to provide comparison data for the computational tools



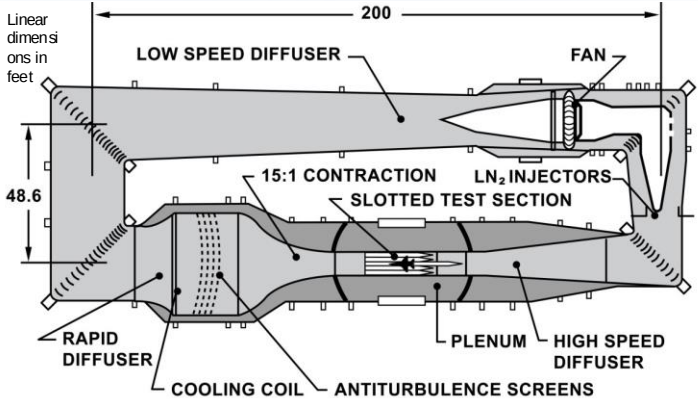
Single Aisle Turboelectric Aircraft Concept with Aft Boundary Layer Ingestion (STARC-ABL)

- **CRM-TCT high Reynolds number experiment in National Transonic Facility**
  - Characterize and measure:
    - Tailcone nacelle inlet pressure and flow angle profile
    - Aftbody boundary layer heights and surface pressures
    - Overall airframe cruise performance
  - Evaluate sensitivity of measured quantities to:
    - Mach number, Reynolds number, angle of attack
    - Mass flow rates through the nacelle
  - Provide comparison dataset for computational tools



Common Research Model with Tail Cone Thruster

National Transonic Facility (NTF)







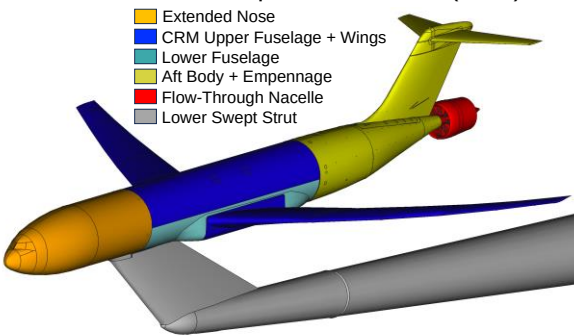
Photos : NASA

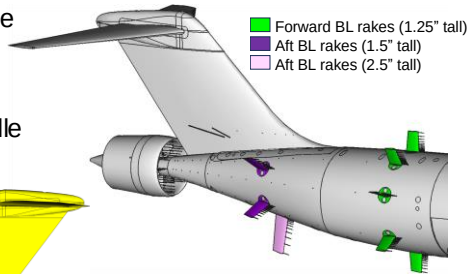
- Located at the NASA Langley Research Center
- Pressurized, cryogenic wind tunnel
- Operate in dry air or gaseous nitrogen
- Achieve very high Reynolds numbers
  - Flight or near-flight for many vehicles

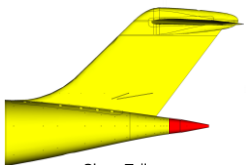
Test Gas	Air	Nitrogen
Mach Number	0.1 – 1.10	0.1 – 1.20
Max Unit Reynolds Number	$20x10^6$ / ft	$145x10^6$ / ft
Total Pressure	1 – 8.3 atm	1 – 8.3 atm
Total Temperature	80°F to 130°F	-250°F to 80°F

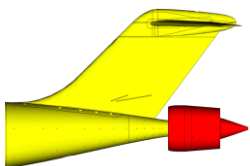
Test Article

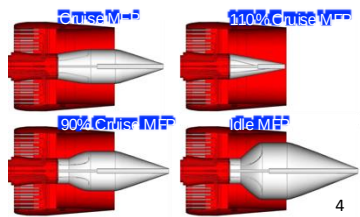
- **Common Research Model with Tail Cone Thruster (CRM-TCT)**
  - 2.7%-scale CRM model with new aftbody and empennage
  - Underchin blade support system
  - Clean tailcone or rotating tailcone nacelles (2)
  - 4 mass flow plugs (MFP) to vary mass flow through nacelle
  - Miniature boundary layer (BL) rakes on aftbody
  - Surface static pressure orifices (>200)






Clean Tailcone


Tailcone Nacelle

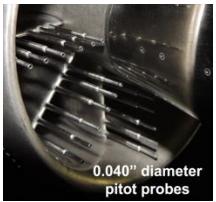


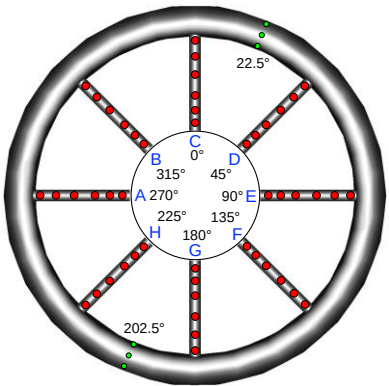
Flow-Through Nacelles

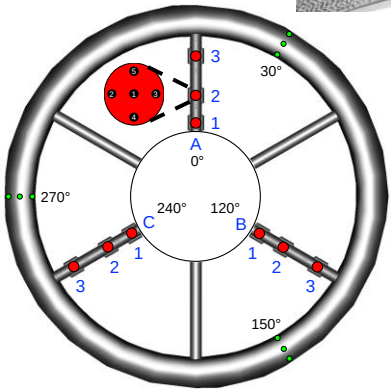
- **ARP1420 nacelle / 5-hole probe nacelle**
  - 3.3” nacelle inlet diameter
  - Measure total pressure and flow angle profile at nacelle highlight
  - Controlled remotely with rotation range between –60º and 60º
  - Operated at tunnel temperatures between –120ºF and 120ºF



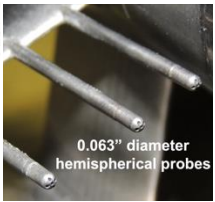
ARP1420 Nacelle





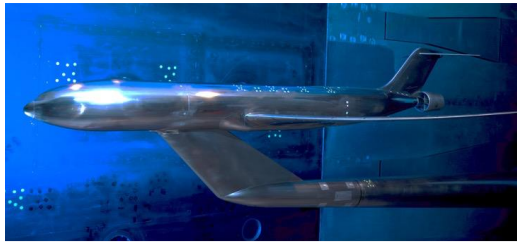


5-hole probe Nacelle



Experiment Setup

- **Test Conditions**
  - M_∞ = 0.75, 0.80, 0.85
  - Re_{mac} = 5M, 10M, 15M
  - T_0 = 120ºF (Air), –50ºF (N_2), –120ºF (N_2)
  - α = -3º to 3º, β = 0º



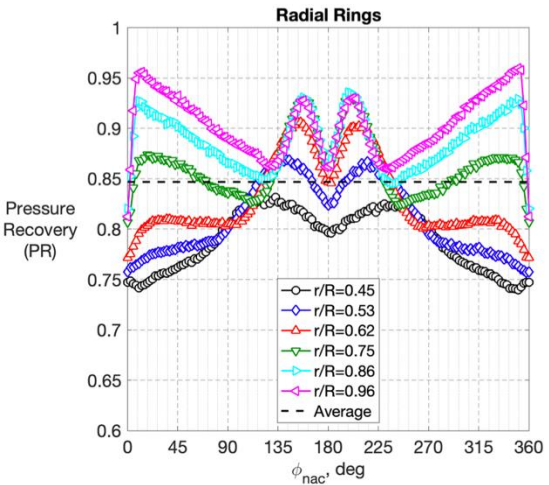
CRM-TCT model in NTF (March – June 2023)

- **Test Matrix**
  - Model configurations
    - Clean tailcone, ARP1420 nacelle, or 5-hole probe nacelle
    - 4 mass flow plugs
    - Horizontal stabilizer on or off
    - Forward or aft BL rakes
  - Data runs
    - Model angle-of-attack traverses at fixed nacelle roll angle
    - Nacelle roll angle rotation at fixed model angle of attack

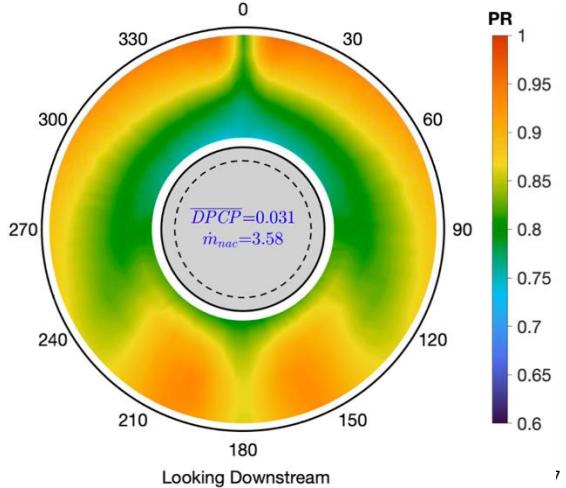
Inlet Flow Distortion (Total Pressure Recovery)

- **Pressure recovery contour**

ARP1420 nacelle with 110% cruise MFP (M_∞ = 0.8, Re_{mac} = 10M, α =



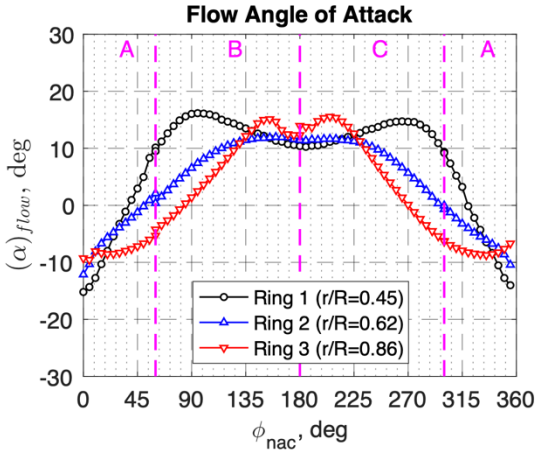
$$PR = \frac{(P_T)_{probe}}{P_0}$$

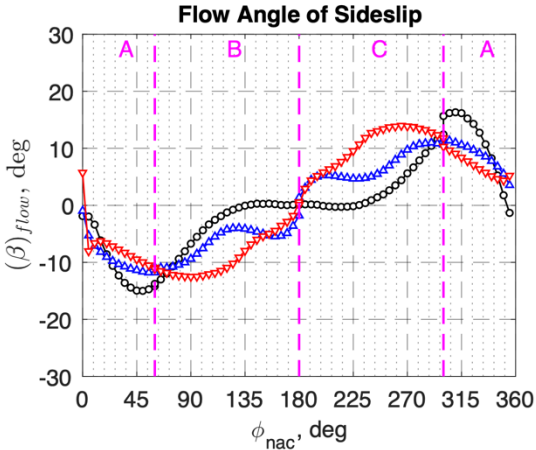


Inlet Flow Distortion (Flow Angle)

- **Data acquired with nacelle rotation in 5º increments over 120º range**
  - Data mostly smooth and symmetric, but some discontinuities at overlap points

5-hole probe nacelle with cruise MFP (M_∞ = 0.8, Re_{mac} = 5M, α = 2º)

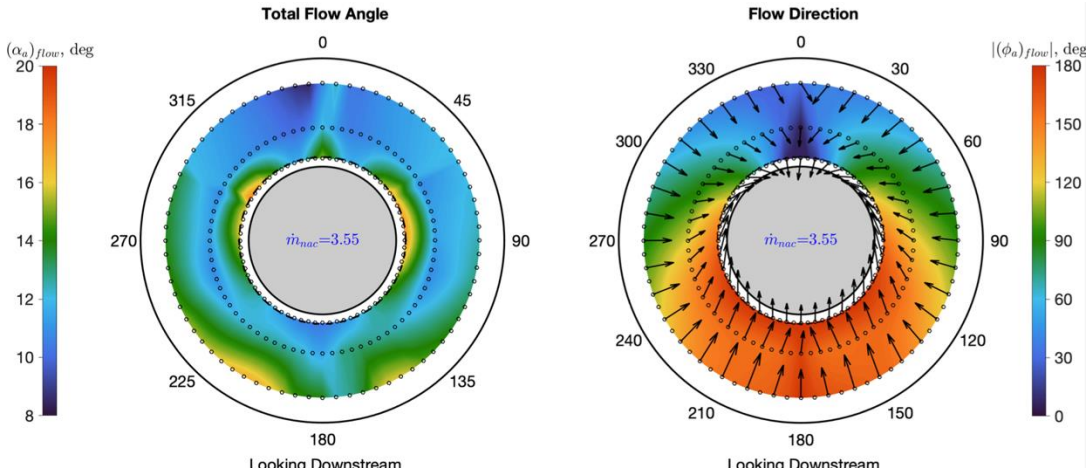




Inlet Flow Distortion (Flow Angle)

- **Flow angle and flow direction contours**
  - Similar features to pressure profile, but also shows rollup around and onto top of hub

5-hole probe nacelle with cruise MFP (M_∞ = 0.8, Re_{mac} = 5M, α = 2º)



Summary

Characterization of TCT inlet pressure and swirl distortion at relevant cruise Mach and Reynolds numbers providing comparison data for PAI CFD capability

- **CRM-TCT test results documented in AIAA paper**
  - D. Chan, et al., "*Experimental Investigation of a Boundary Layer Ingesting Tailcone Thruster Configuration at the National Transonic Facility*", AIAA-2024-3515

- **Test funded by NASA AATT Project**
  - BLITS team comprised of researchers from LaRC, GRC, ARC
  - Thanks to NTF facility team!



The goals of this work are to

- Develop best-practices to simulate BLI flows within the LAVA Curvilinear solver framework using steady RANS
  - Grid refinement study
  - Turbulence model sensitivity study
- Assess the ability of steady RANS to predict the aftbody flow ingested by the TCT
  - Under a variety of conditions
  - Using the experimental data collected for validation

The goals of this work are to

- Develop best-practices to simulate BLI flows within the LAVA Curvilinear solver framework using steady RANS
  - Grid refinement study
  - Turbulence model sensitivity study
- Assess the ability of steady RANS to predict the aftbody flow ingested by the TCT
  - Under a variety of conditions
  - Using the experimental data collected for validation

The goals of this work are to

- Develop best-practices to simulate BLI flows within the LAVA Curvilinear solver framework using steady RANS
  - Grid refinement study
  - Turbulence model sensitivity study
- Assess the ability of steady RANS to predict the aftbody flow ingested by the TCT
  - Under a variety of conditions
  - Using the experimental data collected for validation

The goals of this work are to

- Develop best-practices to simulate BLI flows within the LAVA Curvilinear solver framework using steady RANS
  - Grid refinement study
  - Turbulence model sensitivity study
- Assess the ability of steady RANS to predict the aftbody flow ingested by the TCT
  - Under a variety of conditions
  - Using the experimental data collected for validation

Modeling the problem

LAVA Launch, Ascent, and Vehicle Aerodynamics

- Several grid paradigms: curvilinear overset, unstructured, cartesian
- Conservative finite-difference formulation of the RANS equations

Modeling the problem

LAVA Launch, Ascent, and Vehicle Aerodynamics

- Several grid paradigms: curvilinear overset, unstructured, cartesian
- Conservative finite-difference formulation of the RANS equations
- Turbulence closure: SA w/ RC and QCR corrections (SA-RC-QCR2000)

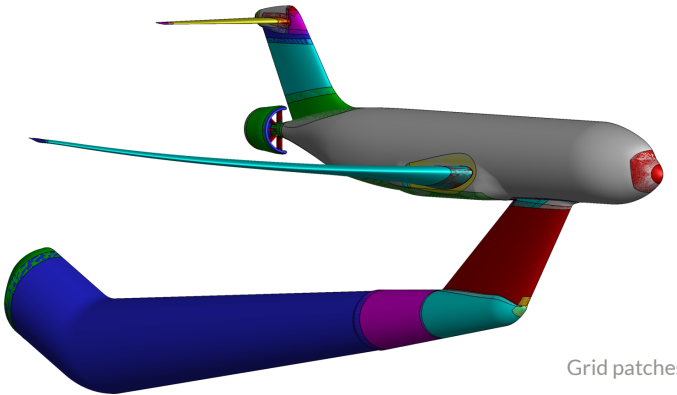
Modeling the problem

LAVA Launch, Ascent, and Vehicle Aerodynamics

- Several grid paradigms: curvilinear overset, unstructured, cartesian
- Conservative finite-difference formulation of the RANS equations
- Turbulence closure: SA w/ RC and QCR corrections (SA-RC-QCR2000)
- Convective fluxes
  - Modified Roe scheme w/ third-order left/right state reconstruction
  - Koren limiter

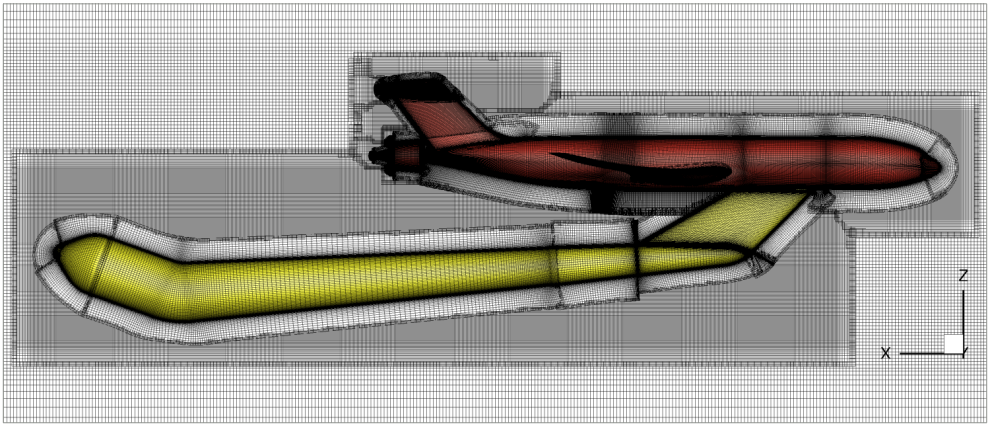
Computational setup

- Half-span model with symmetry BC at Y = 0[m]
- Viscous wall BC applied at model surfaces



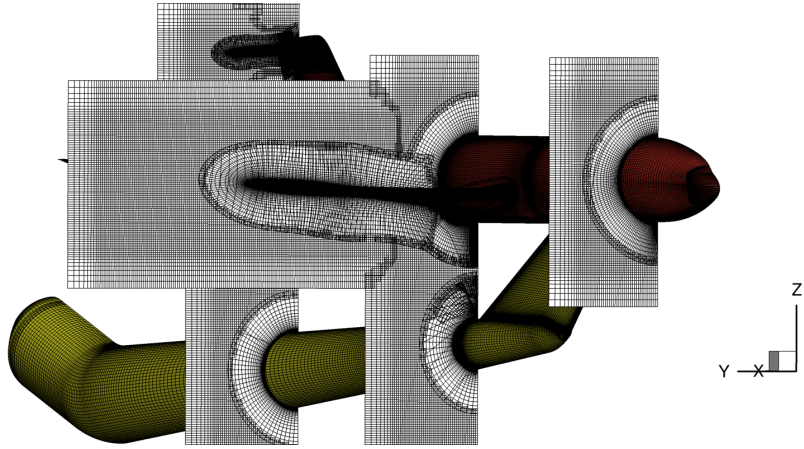
Grid patches overview

Overview of the grid system



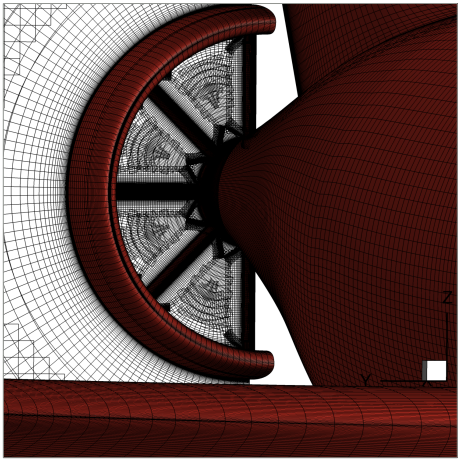
Grid slice side view. Configuration: *Flow-through w/ Cruise MFP (w/ sting)*

Overview of the grid system

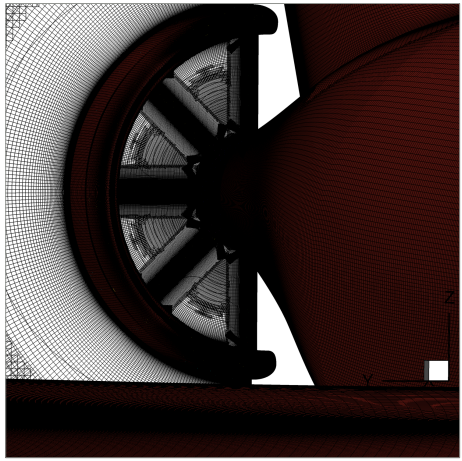


Grid slices. Configuration: *Flow-through w/ Cruise MFP (w/ sting)*

Overview of the grid system

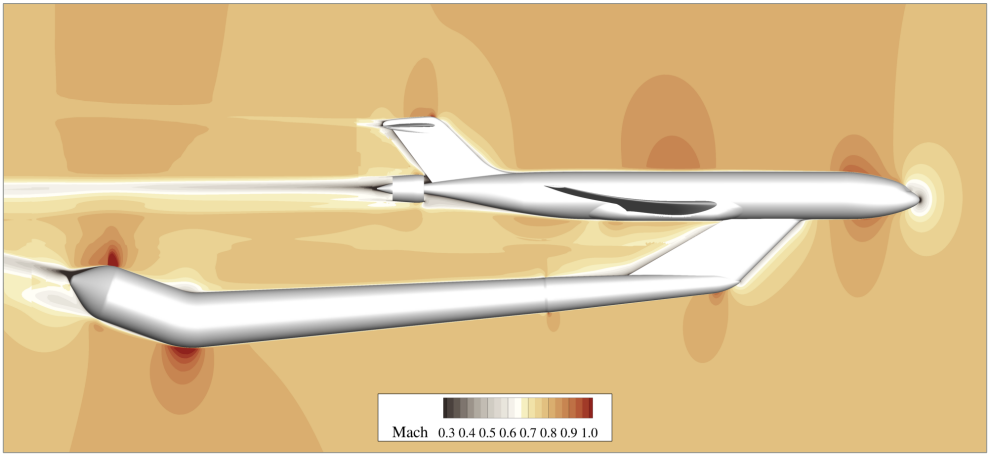


Coarse grid



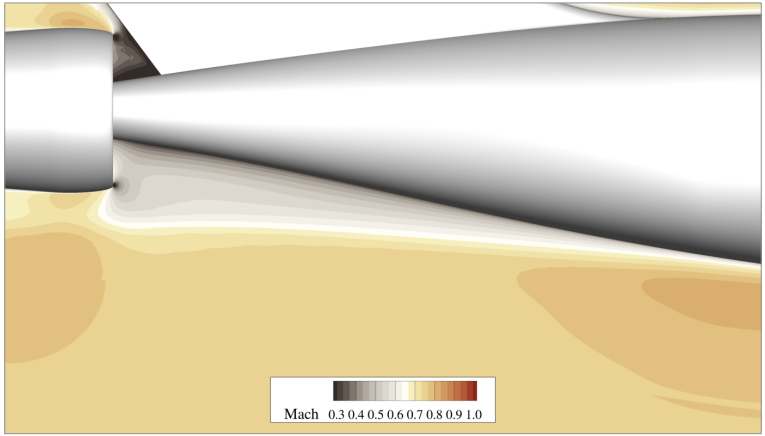
Extra fine grid

Flow-field overview



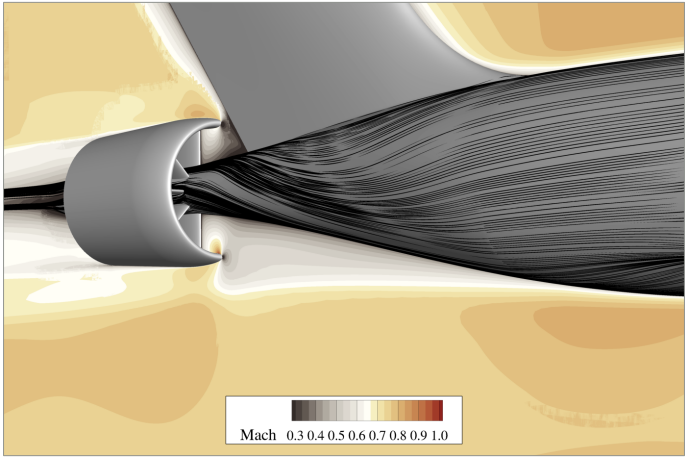
Flow-field side-view showing Mach number contours.

Flow-field overview



Flow-field side-view showing Mach number contours.

Flow-field overview



Flow-field side-view showing Mach number contours.

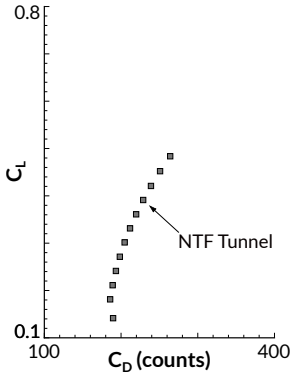
Grid refinement study results

	Coarse	Medium	Fine	Extra Fine
# Grid Points (millions)	49.6	116.9	276.4	685.3

Grid refinement study results

	Coarse	Medium	Fine	Extra Fine
# Grid Points (millions)	49.6	116.9	276.4	685.3

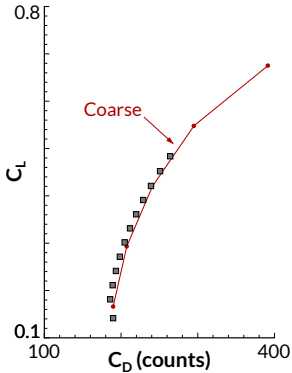
Re = 5-million
Ma = 0.80



Grid refinement study results

	Coarse	Medium	Fine	Extra Fine
# Grid Points (millions)	49.6	116.9	276.4	685.3

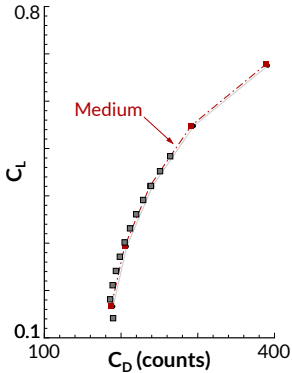
Re = 5-million
Ma = 0.80



Grid refinement study results

	Coarse	Medium	Fine	Extra Fine
# Grid Points (millions)	49.6	116.9	276.4	685.3

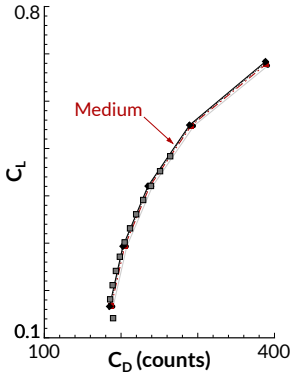
Re = 5-million
Ma = 0.80



Grid refinement study results

	Coarse	Medium	Fine	Extra Fine
# Grid Points (millions)	49.6	116.9	276.4	685.3

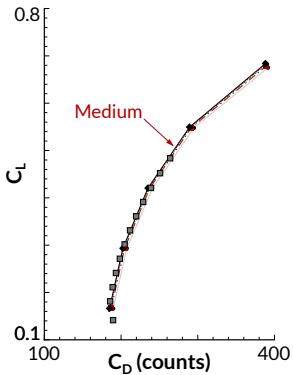
Re = 5-million
Ma = 0.80

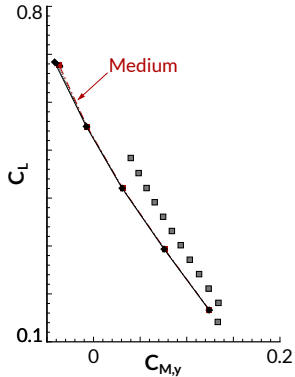


Grid refinement study results

	Coarse	Medium	Fine	Extra Fine
# Grid Points (millions)	49.6	116.9	276.4	685.3

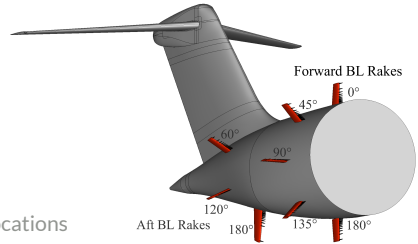
Re = 5-million
Ma = 0.80



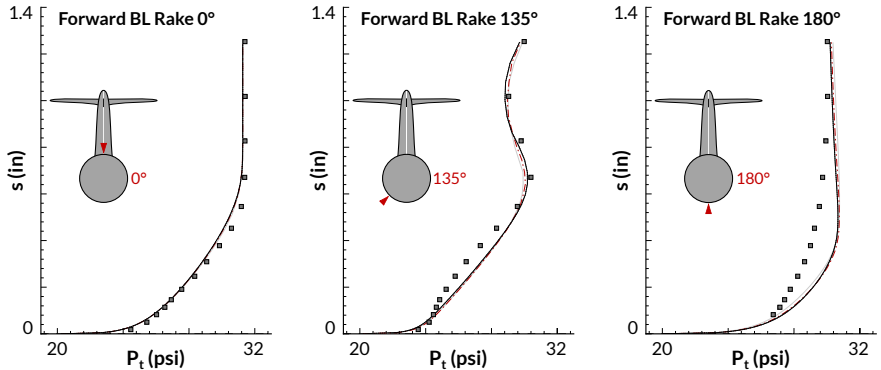


Grid refinement study results

Re = 5-million, Ma = 0.80, α = 2°

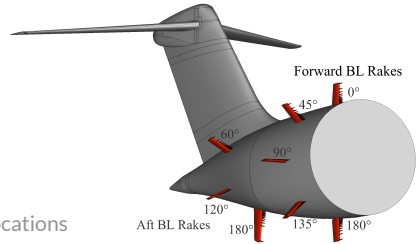


Boundary layer rakes locations



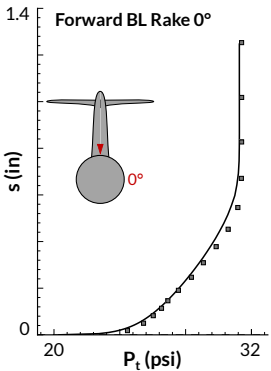
Turbulence model sensitivity

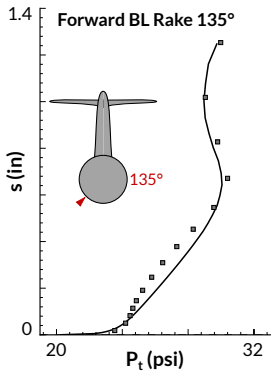
Re = 5-million, Ma = 0.80, α = 2°

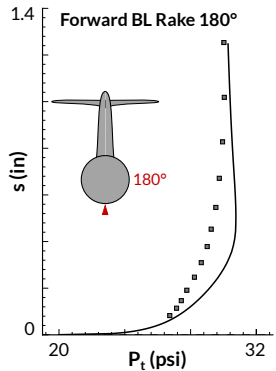


Boundary layer rakes locations

NTF Tunnel
SA-RC-QCR2000

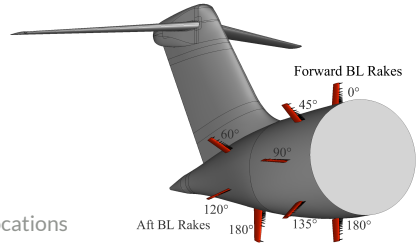






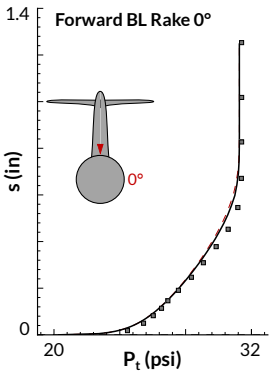
Turbulence model sensitivity

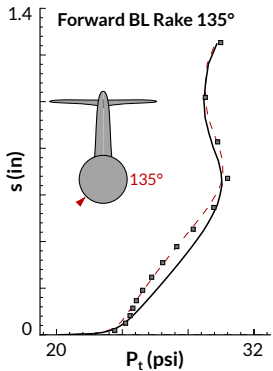
Re = 5-million, Ma = 0.80, α = 2°

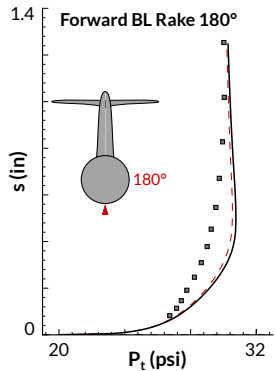


Boundary layer rakes locations

- NTF Tunnel
- SA-RC-QCR2000
- SA

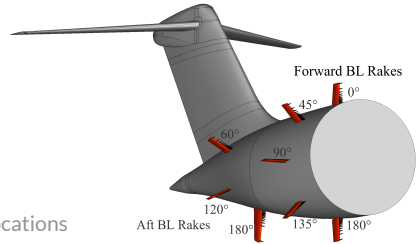






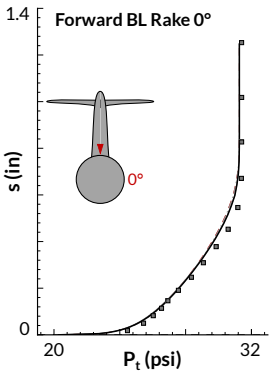
Turbulence model sensitivity

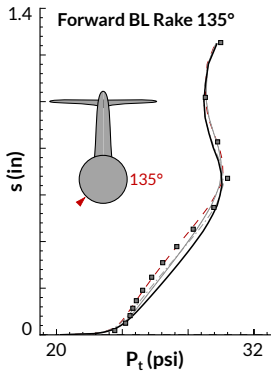
Re = 5-million, Ma = 0.80, α = 2°

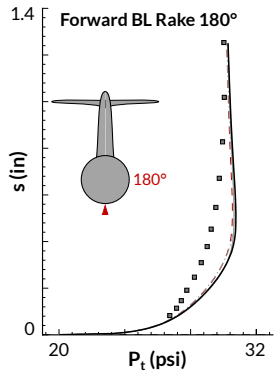


Boundary layer rakes locations

- NTF Tunnel
- SA-RC-QCR2000
- SA
- SA-RC
- SA-QCR2000

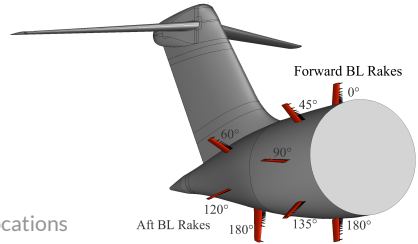






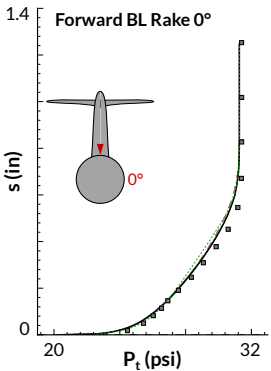
Turbulence model sensitivity

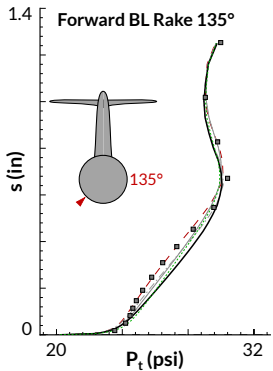
Re = 5-million, Ma = 0.80, α = 2°

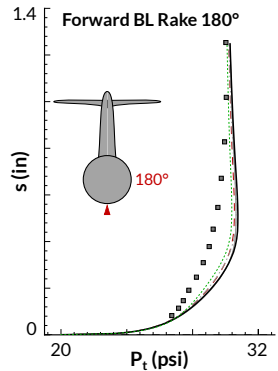


Boundary layer rakes locations

- NTF Tunnel
- SA-RC-QCR2000
- SA
- SA-RC
- SA-QCR2000
- k-w BSL

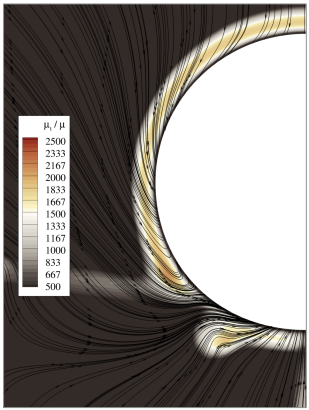


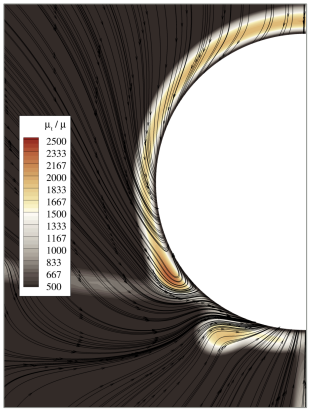


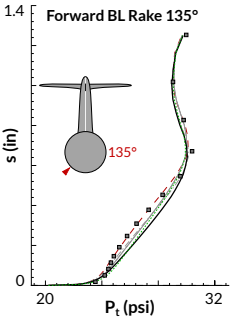


Turbulence model sensitivity

Re = 5-million, Ma = 0.80, α = 2°







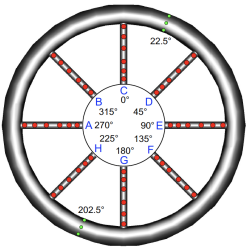
SA-RC-QCR2000

SA

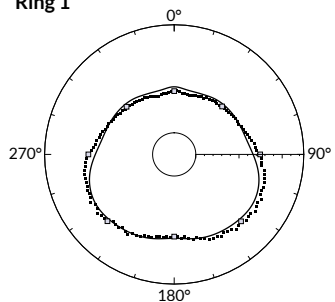
Turbulence model sensitivity

Re = 10-million, Ma = 0.80, α = 2°

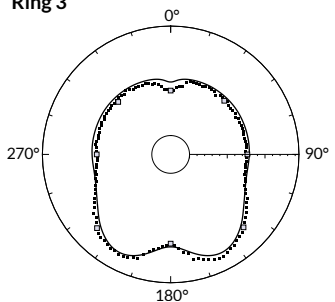
ARP1420 probe locations
(Credit: Chan, D., 2024)



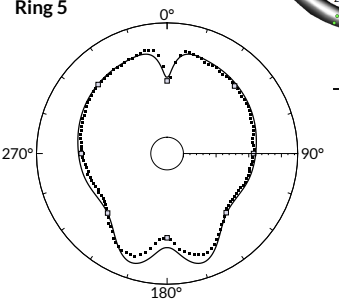
Ring 1



Ring 3



Ring 5

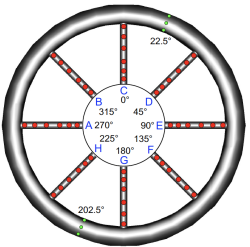


NTF Tunnel
SA-RC-QCR2000

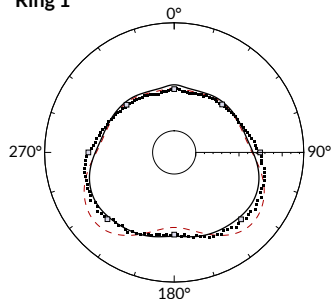
Turbulence model sensitivity

Re = 10-million, Ma = 0.80, α = 2°

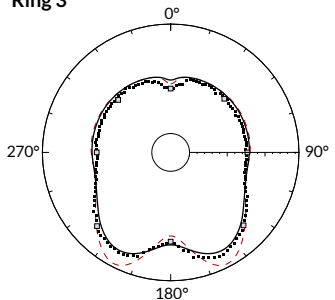
ARP1420 probe locations
(Credit: Chan, D., 2024)



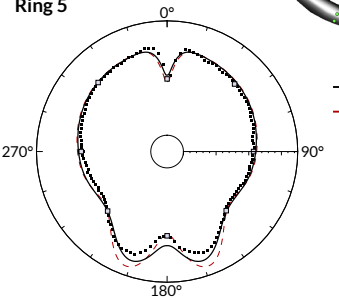
Ring 1



Ring 3



Ring 5

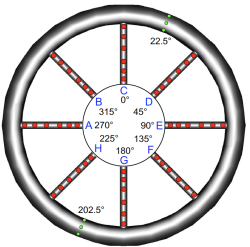


- NTF Tunnel
- SA-RC-QCR2000
- SA

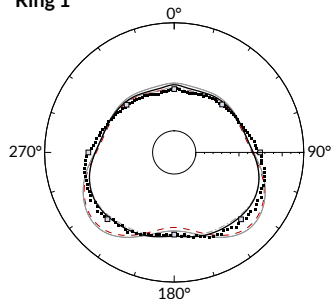
Turbulence model sensitivity

Re = 10-million, Ma = 0.80, α = 2°

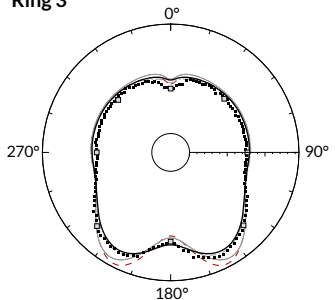
ARP1420 probe locations
(Credit: Chan, D., 2024)



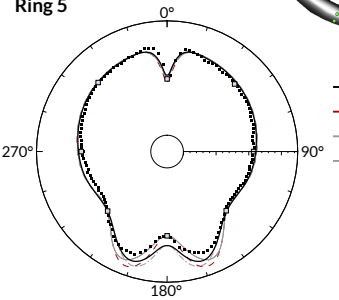
Ring 1



Ring 3



Ring 5

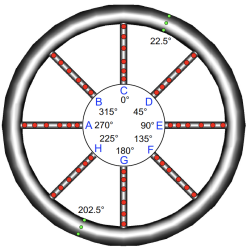


- NTF Tunnel
- SA-RC-QCR2000
- SA
- SA-RC
- SA-QCR2000

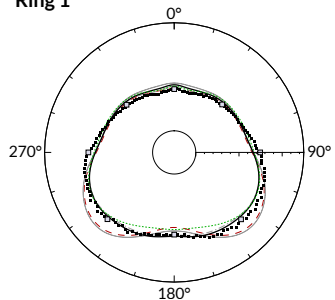
Turbulence model sensitivity

Re = 10-million, Ma = 0.80, α = 2°

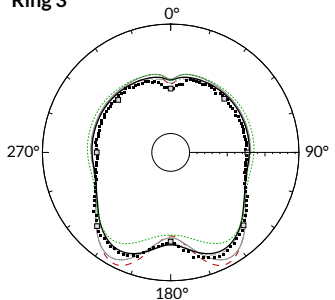
ARP1420 probe locations
(Credit: Chan, D., 2024)



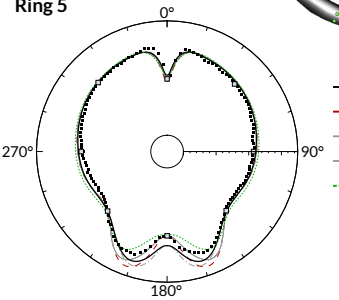
Ring 1



Ring 3



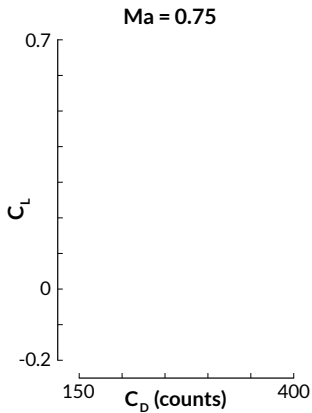
Ring 5



- NTF Tunnel
- SA-RC-QCR2000
- SA
- SA-RC
- SA-QCR2000
- k-w BSL

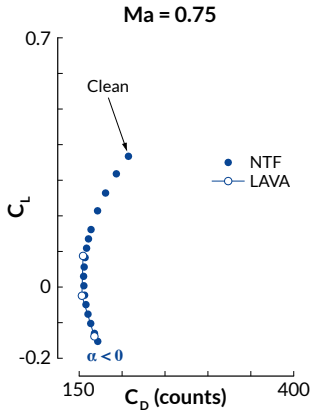
Results - Load coefficients

Re = 5-million



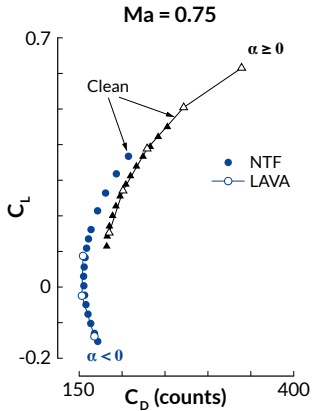
Results - Load coefficients

Re = 5-million



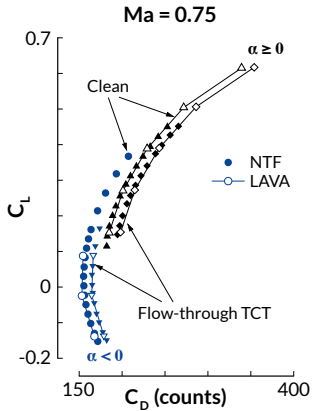
Results - Load coefficients

Re = 5-million



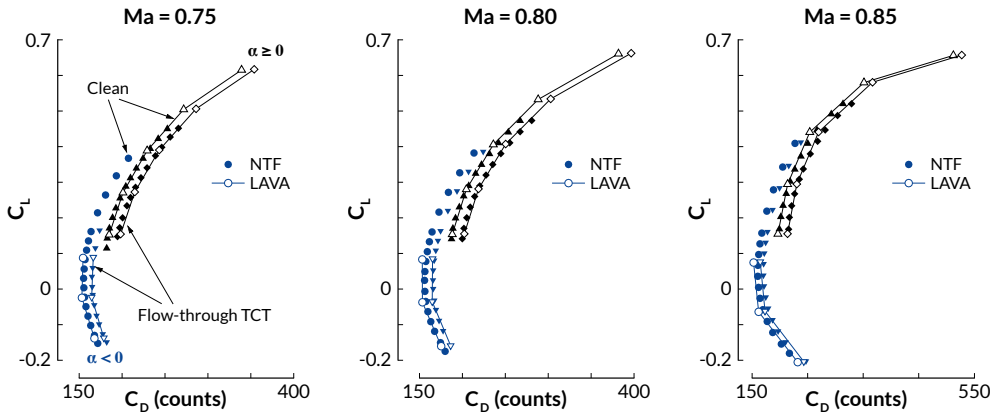
Results - Load coefficients

Re = 5-million



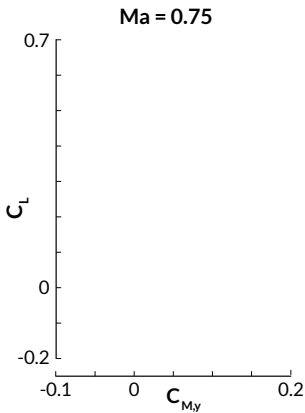
Results - Load coefficients

Re = 5-million



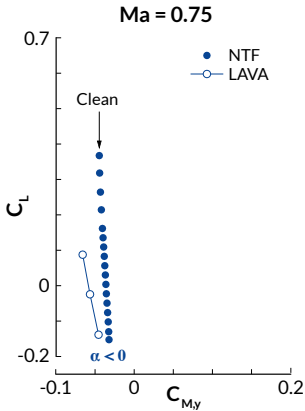
Results - Load coefficients

Re = 5-million



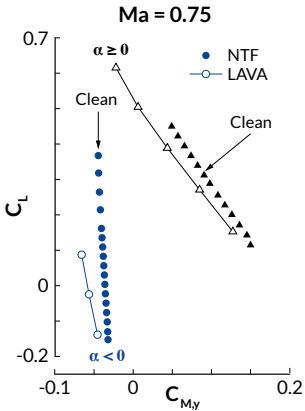
Results - Load coefficients

Re = 5-million



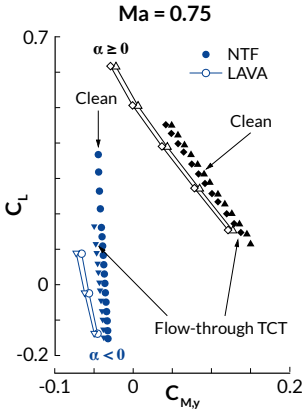
Results - Load coefficients

Re = 5-million



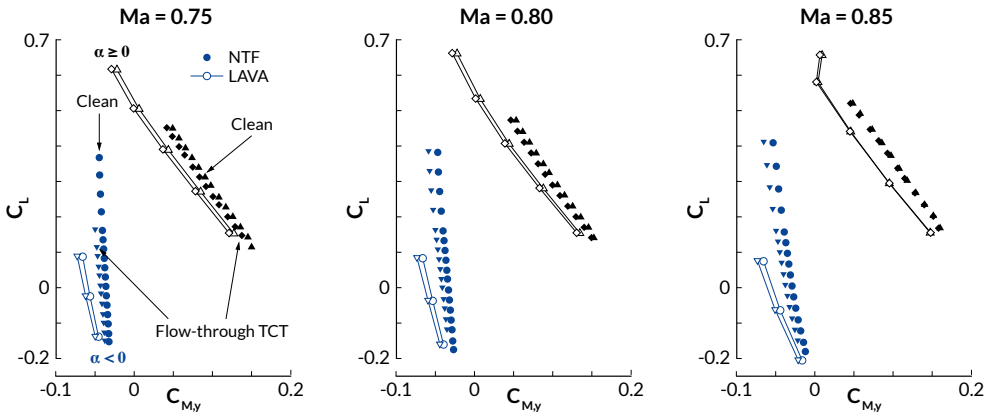
Results - Load coefficients

Re = 5-million



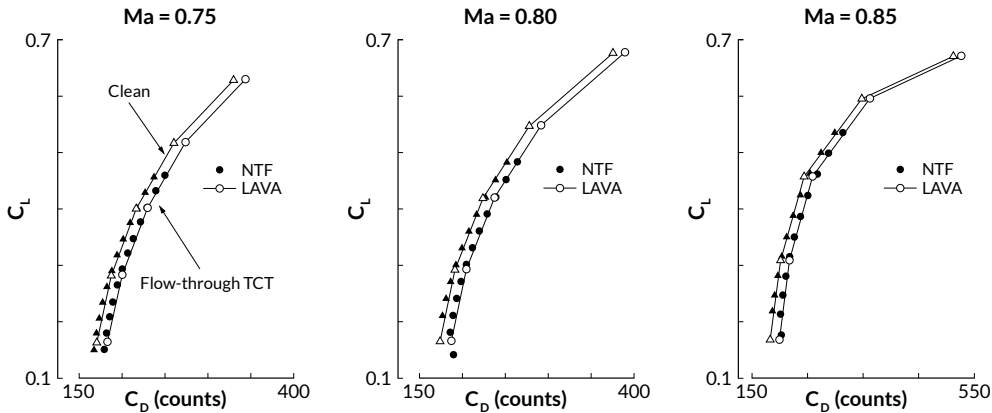
Results - Load coefficients

Re = 5-million



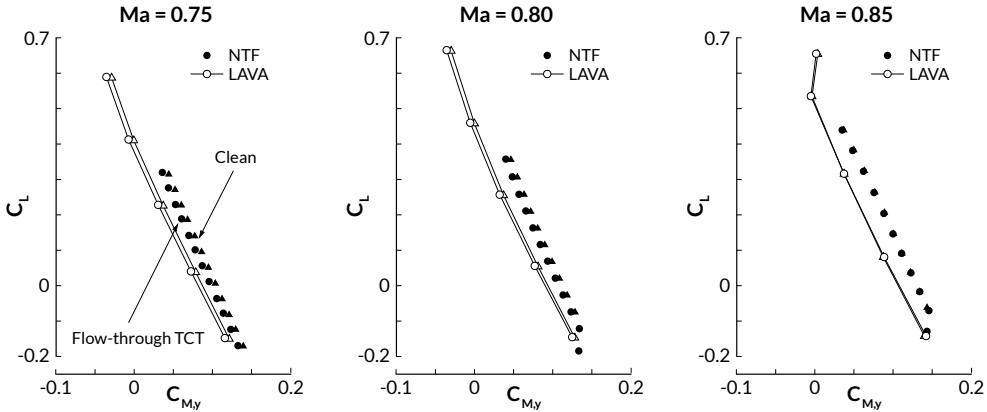
Results - Load coefficients

Re = 10-million



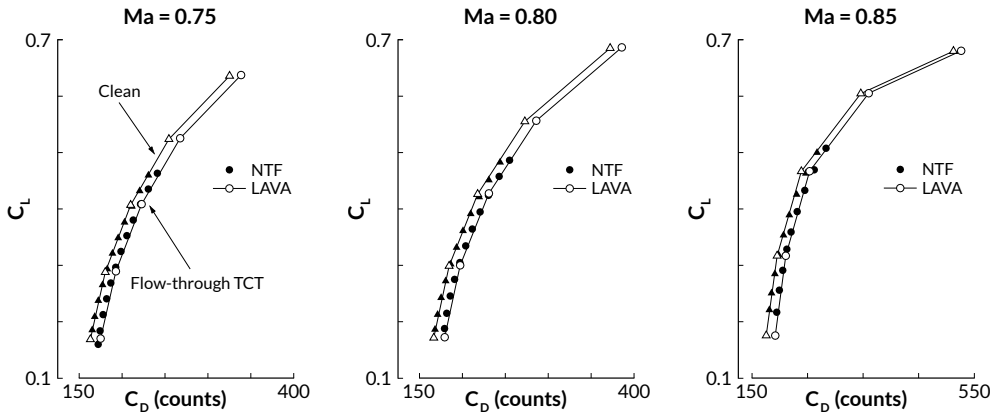
Results - Load coefficients

Re = 10-million



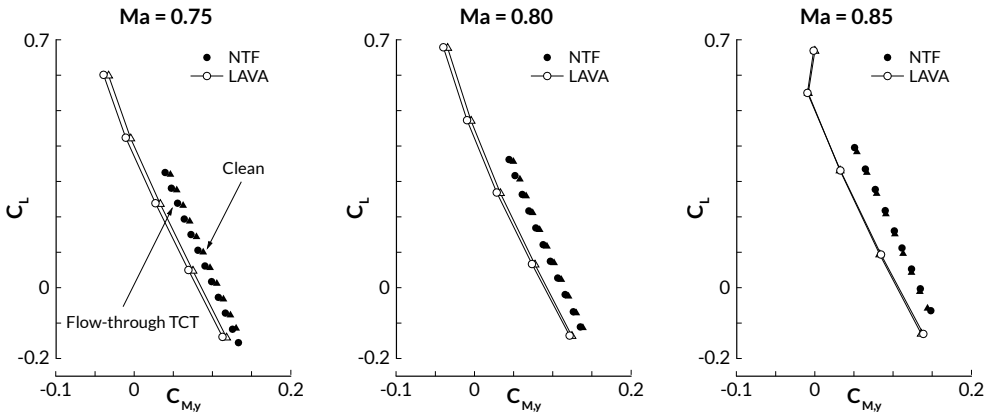
Results - Load coefficients

Re = 15-million



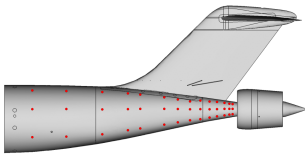
Results - Load coefficients

Re = 15-million

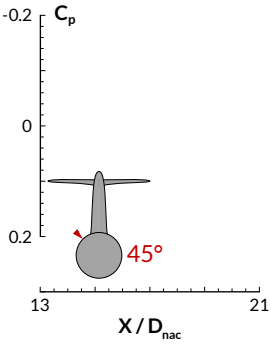


Results - Aftbody surface pressures

Re = 5-million, Ma = 0.80, α = 2°

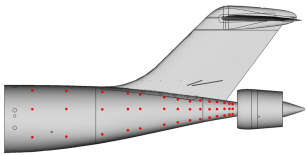


5-hole probe locations
(Credit: Chan, D., 2024)

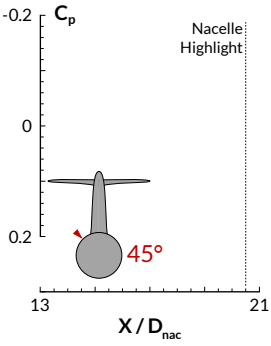


Results - Aftbody surface pressures

Re = 5-million, Ma = 0.80, α = 2°

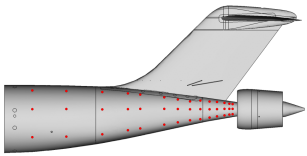


5-hole probe locations
(Credit: Chan, D., 2024)

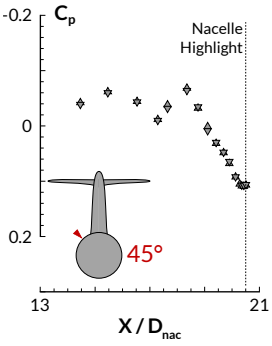


Results - Aftbody surface pressures

Re = 5-million, Ma = 0.80, α = 2°

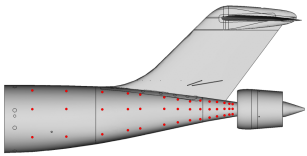


5-hole probe locations
(Credit: Chan, D., 2024)

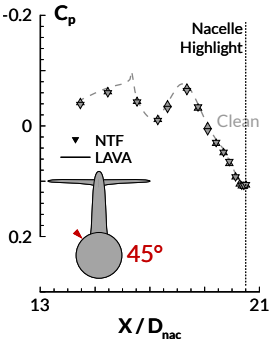


Results - Aftbody surface pressures

Re = 5-million, Ma = 0.80, α = 2°

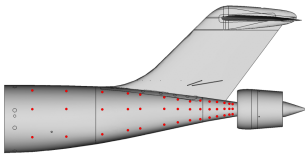


5-hole probe locations
(Credit: Chan, D., 2024)

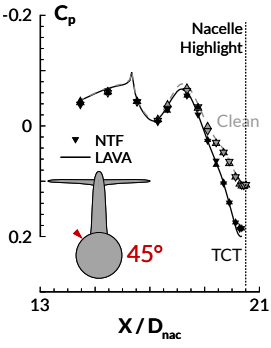


Results - Aftbody surface pressures

Re = 5-million, Ma = 0.80, α = 2°

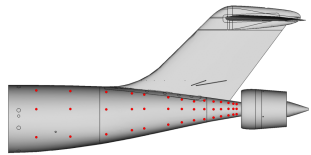


5-hole probe locations
(Credit: Chan, D., 2024)

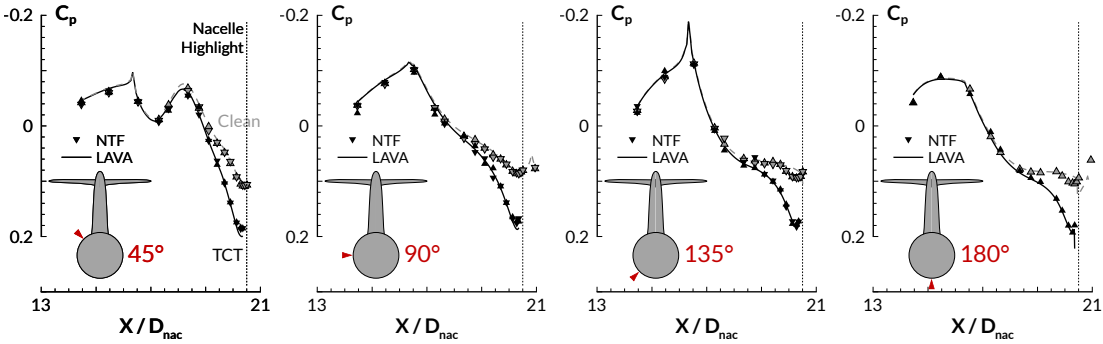


Results - Aftbody surface pressures

Re = 5-million, Ma = 0.80, α = 2°

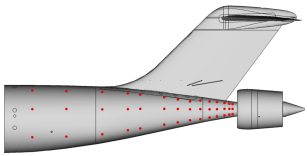


5-hole probe locations
(Credit: Chan, D., 2024)

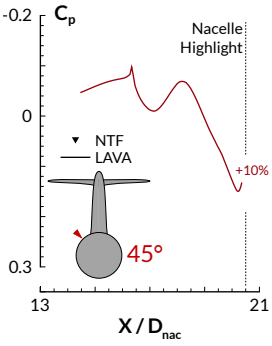


Results - Aftbody surface pressures

Re = 5-million, Ma = 0.80, α = 2°

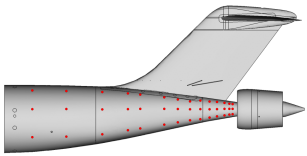


5-hole probe locations
(Credit: Chan, D., 2024)

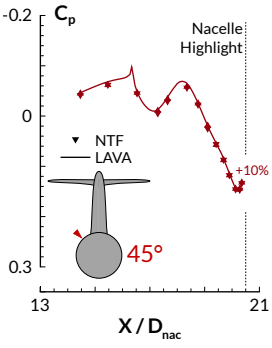


Results - Aftbody surface pressures

Re = 5-million, Ma = 0.80, α = 2°

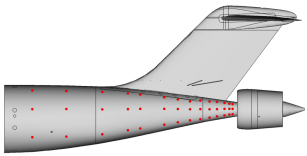


5-hole probe locations
(Credit: Chan, D., 2024)

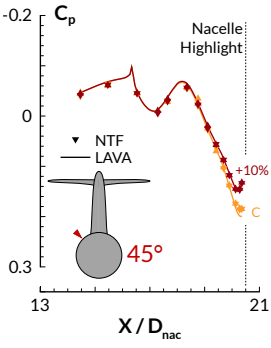


Results - Aftbody surface pressures

Re = 5-million, Ma = 0.80, α = 2°

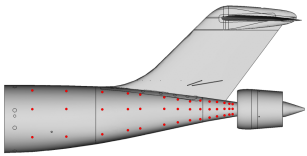


5-hole probe locations
(Credit: Chan, D., 2024)

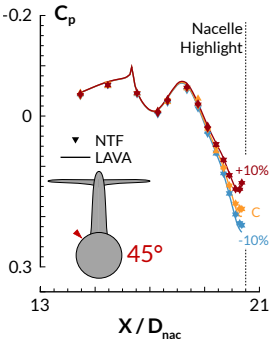


Results - Aftbody surface pressures

Re = 5-million, Ma = 0.80, α = 2°

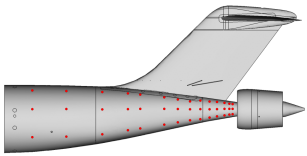


5-hole probe locations
(Credit: Chan, D., 2024)

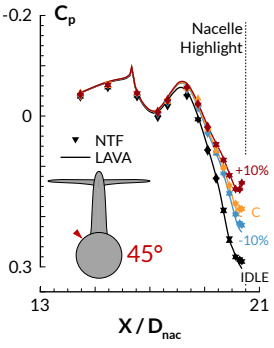


Results - Aftbody surface pressures

Re = 5-million, Ma = 0.80, α = 2°

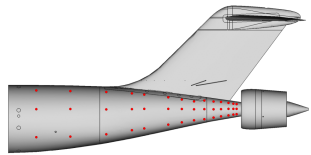


5-hole probe locations
(Credit: Chan, D., 2024)

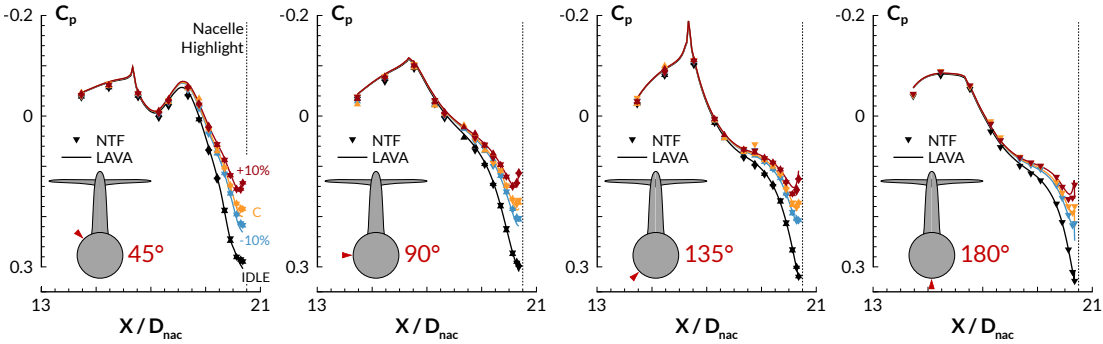


Results - Aftbody surface pressures

Re = 5-million, Ma = 0.80, α = 2°



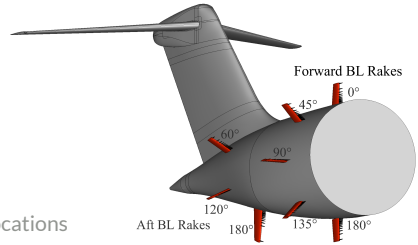
5-hole probe locations
(Credit: Chan, D., 2024)



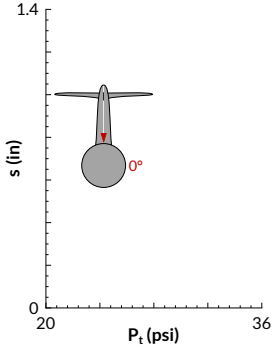
Results - Boundary layer rakes

Re = 5-million, Ma = 0.85

Front rakes



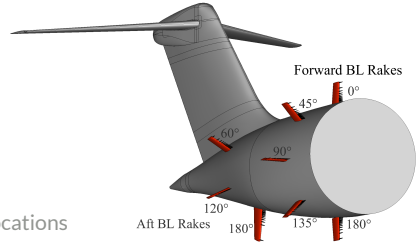
Boundary layer rakes locations



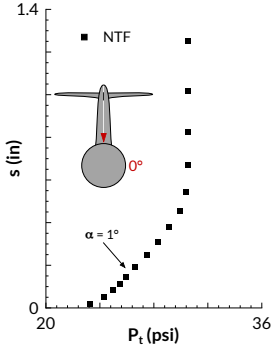
Results - Boundary layer rakes

Re = 5-million, Ma = 0.85, α = 1°

Front rakes



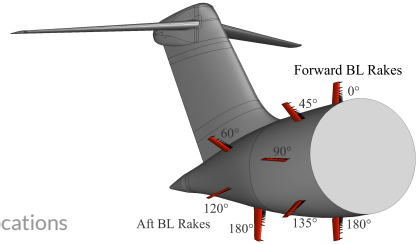
Boundary layer rakes locations



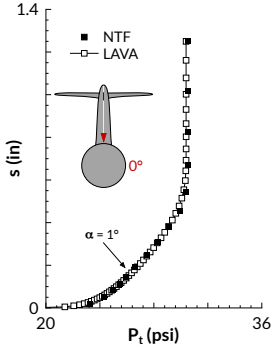
Results - Boundary layer rakes

Re = 5-million, Ma = 0.85, α = 1°

Front rakes



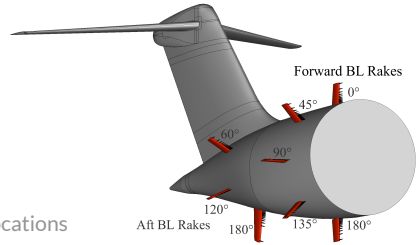
Boundary layer rakes locations



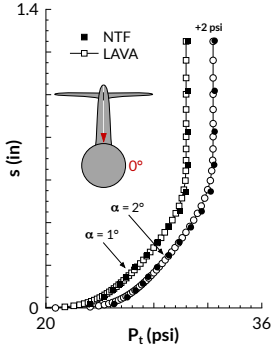
Results - Boundary layer rakes

Re = 5-million, Ma = 0.85, α = 1°, 2°

Front rakes



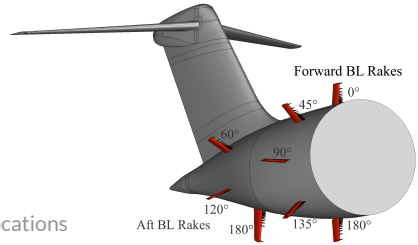
Boundary layer rakes locations



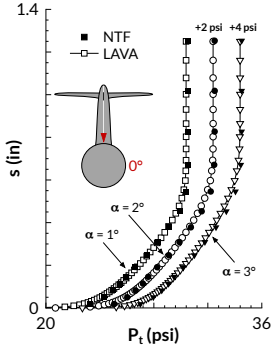
Results - Boundary layer rakes

Re = 5-million, Ma = 0.85, α = 1°, 2°, 3°

Front rakes



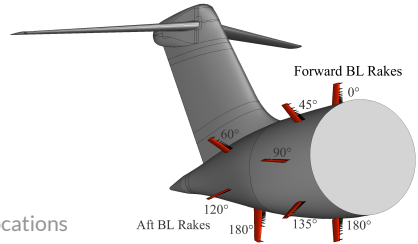
Boundary layer rakes locations



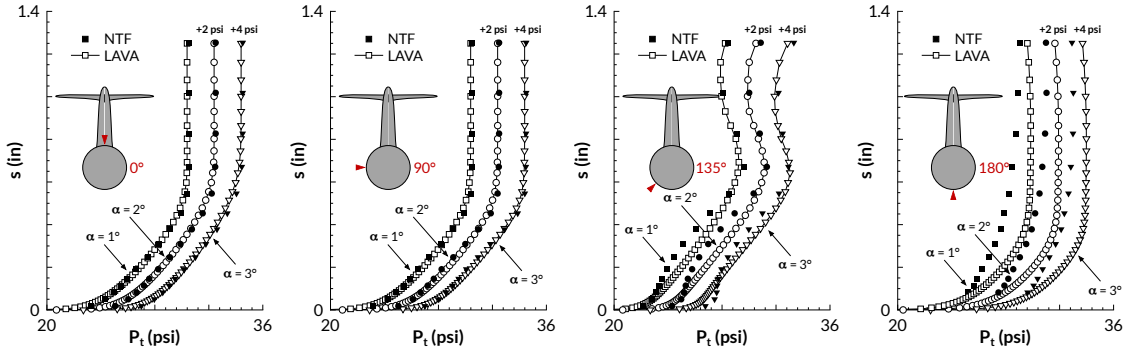
Results - Boundary layer rakes

Re = 5-million, Ma = 0.85, α = 1°, 2°, 3°

Front rakes



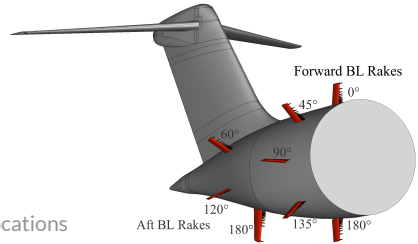
Boundary layer rakes locations



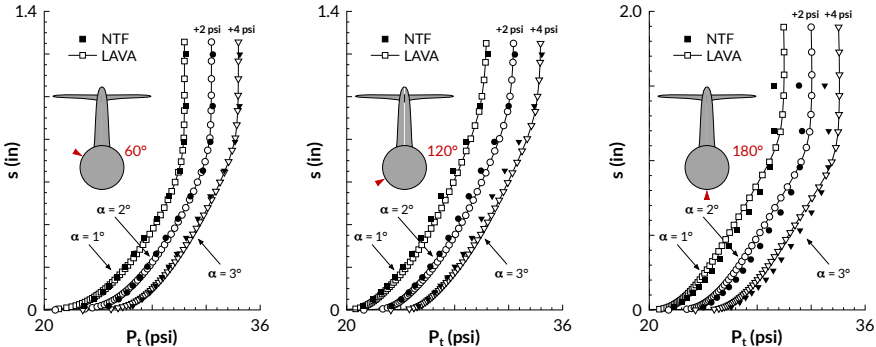
Results - Boundary layer rakes

Re = 5-million, Ma = 0.85, α = 1°, 2°, 3°

Aft rakes



Boundary layer rakes locations

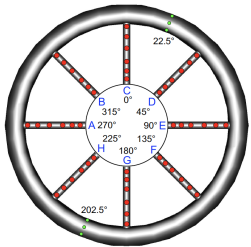


Results - Nacelle highlight total pressure distortion

Re = 5-million, Ma = 0.75, α = 2°

Pressure Recovery = $\frac{P_t}{P_{t,\infty}}$

ARP1420 probe locations
(Credit: Chan, D., 2024)

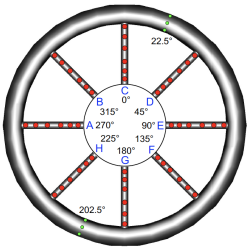


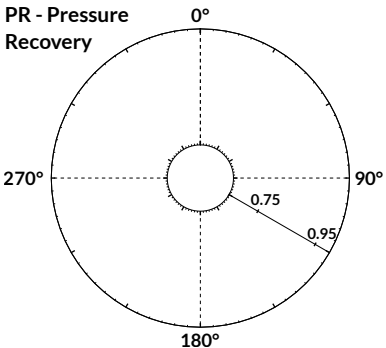
Results - Nacelle highlight total pressure distortion

Re = 5-million, Ma = 0.75, α = 2°

Pressure Recovery = $\frac{P_t}{P_{t,\infty}}$

ARP1420 probe locations
(Credit: Chan, D., 2024)



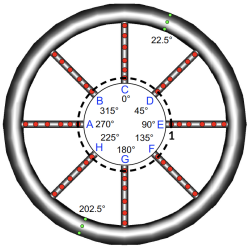


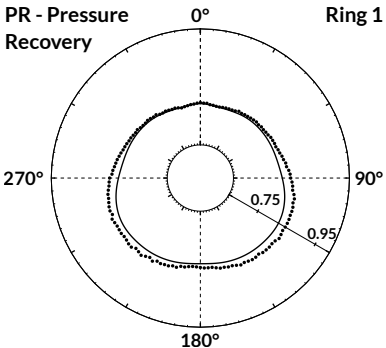
Results - Nacelle highlight total pressure distortion

Re = 5-million, Ma = 0.75, α = 2°

Pressure Recovery = $\frac{P_t}{P_{t,\infty}}$

ARP1420 probe locations
(Credit: Chan, D., 2024)



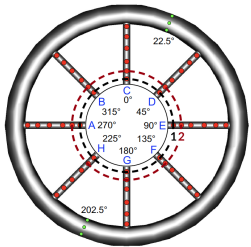


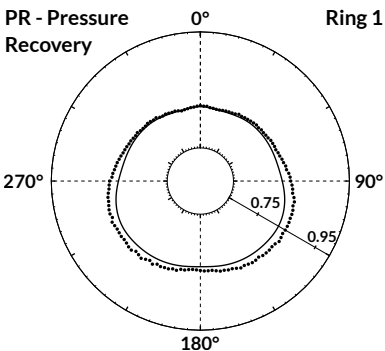
Results - Nacelle highlight total pressure distortion

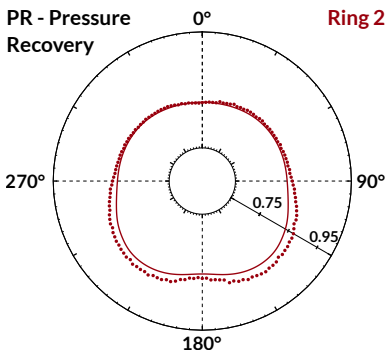
Re = 5-million, Ma = 0.75, $\alpha = 2^\circ$

Pressure Recovery = $\frac{P_t}{P_{t,\infty}}$

ARP1420 probe locations
(Credit: Chan, D., 2024)





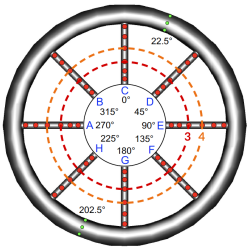


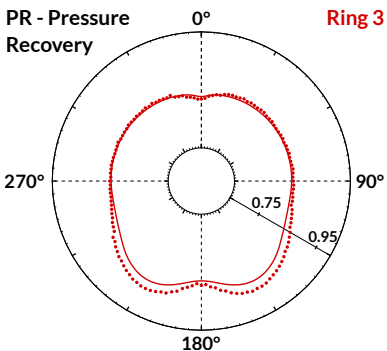
Results - Nacelle highlight total pressure distortion

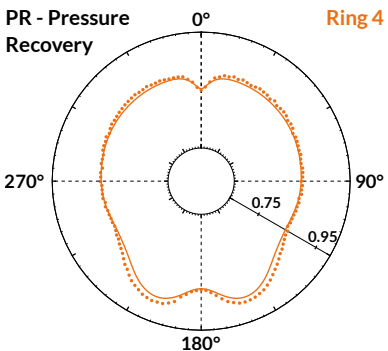
Re = 5-million, Ma = 0.75, $\alpha = 2^\circ$

Pressure Recovery = $\frac{P_t}{P_{t,\infty}}$

ARP1420 probe locations
(Credit: Chan, D., 2024)





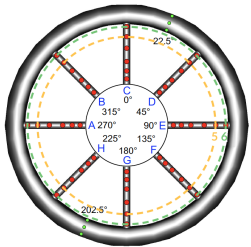


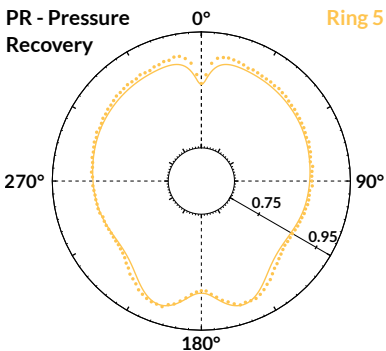
Results - Nacelle highlight total pressure distortion

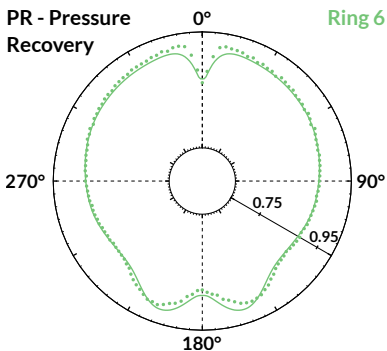
Re = 5-million, Ma = 0.75, $\alpha = 2^\circ$

Pressure Recovery = $\frac{P_t}{P_{t,\infty}}$

ARP1420 probe locations
(Credit: Chan, D., 2024)



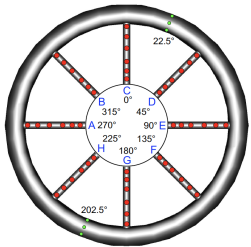


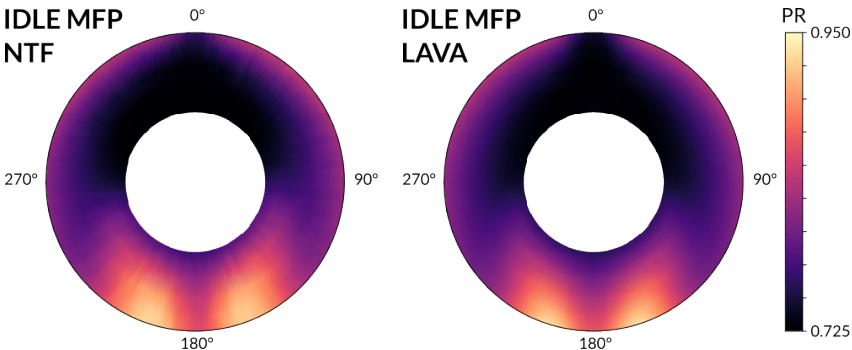


Results - Nacelle highlight total pressure distortion

Re = 5-million, Ma = 0.85, α = 2°
Mass flow plug (MFP) effects

ARP1420 probe locations
(Credit: Chan, D., 2024)

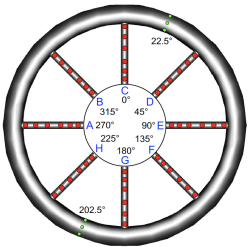


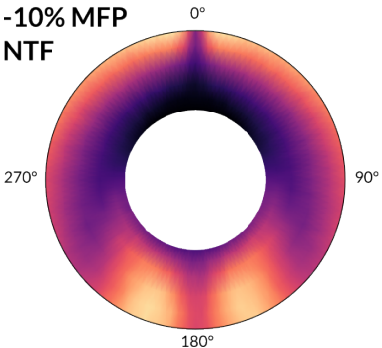


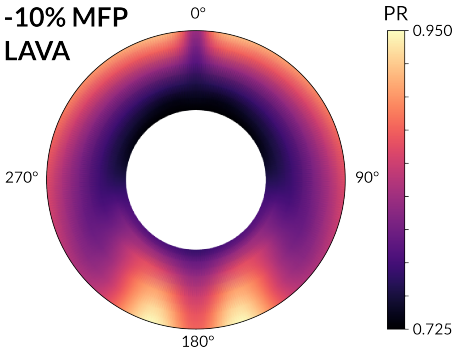
Results - Nacelle highlight total pressure distortion

Re = 5-million, Ma = 0.85, α = 2°
Mass flow plug (MFP) effects

ARP1420 probe locations
(Credit: Chan, D., 2024)



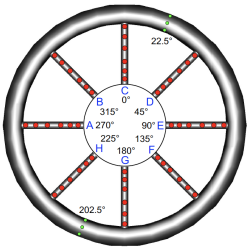


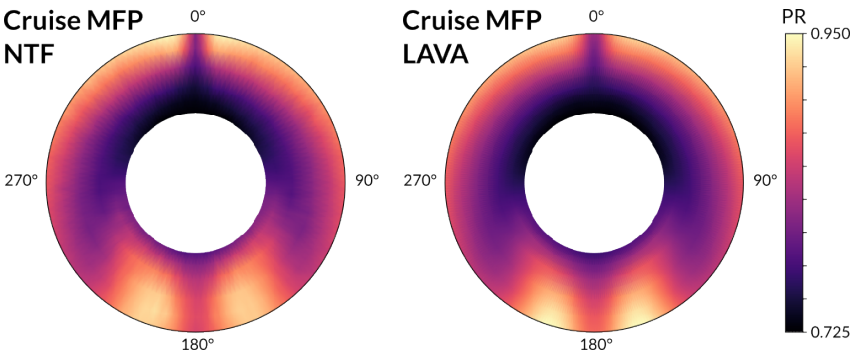


Results - Nacelle highlight total pressure distortion

Re = 5-million, Ma = 0.85, α = 2°
Mass flow plug (MFP) effects

ARP1420 probe locations
(Credit: Chan, D., 2024)

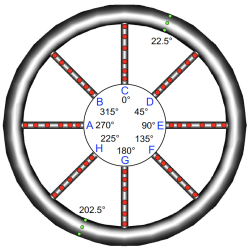


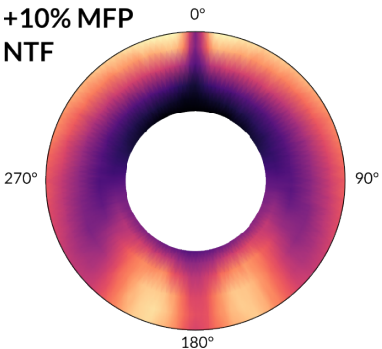


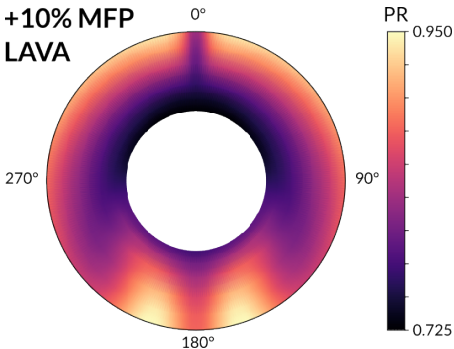
Results - Nacelle highlight total pressure distortion

Re = 5-million, Ma = 0.85, α = 2°
Mass flow plug (MFP) effects

ARP1420 probe locations
(Credit: Chan, D., 2024)





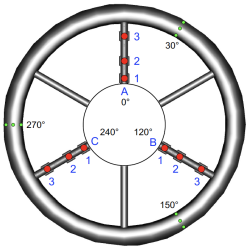


Results - Nacelle highlight flow angularity distortion

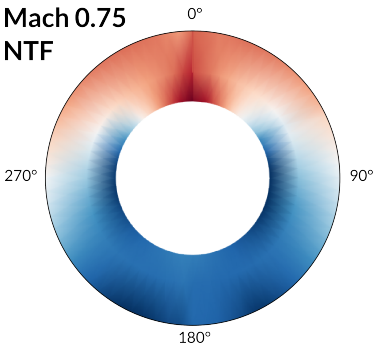
Re = 5-million, α = 2°

Mach number effects

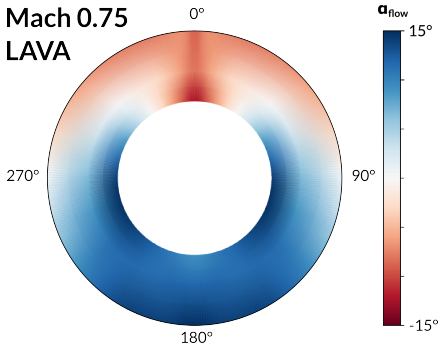
5-hole probe locations
(Credit: Chan, D., 2024)



Mach 0.75
NTF



Mach 0.75
LAVA



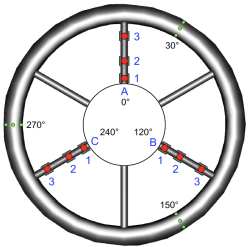
$$\alpha_{\text{flow}} = \operatorname{atan} \frac{V_z}{V_x}$$

Results - Nacelle highlight flow angularity distortion

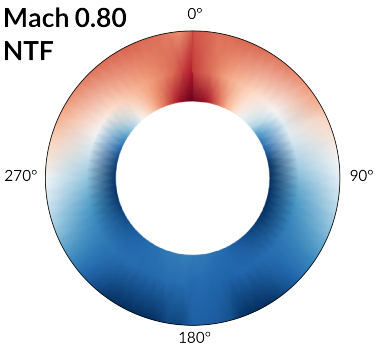
Re = 5-million, α = 2°

Mach number effects

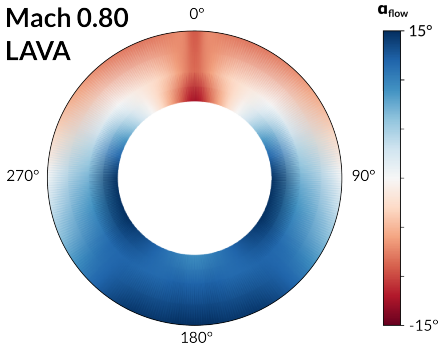
5-hole probe locations
(Credit: Chan, D., 2024)



Mach 0.80
NTF



Mach 0.80
LAVA



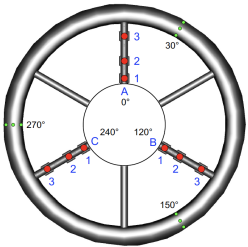
$$\alpha_{\text{flow}} = \operatorname{atan} \frac{V_z}{V_x}$$

Results - Nacelle highlight flow angularity distortion

Re = 5-million, α = 2°

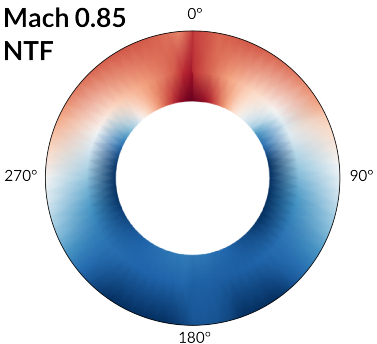
Mach number effects

5-hole probe locations
(Credit: Chan, D., 2024)

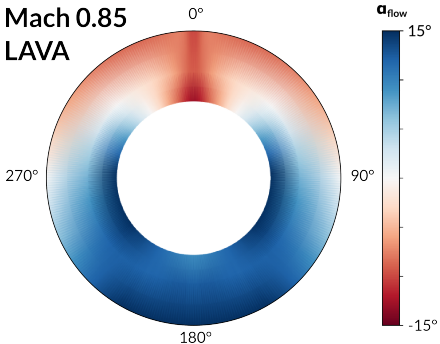


$$\alpha_{\text{flow}} = \operatorname{atan} \frac{V_z}{V_x}$$

Mach 0.85
NTF



Mach 0.85
LAVA

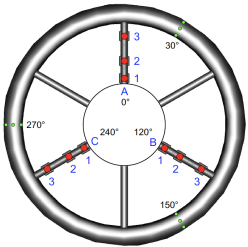


Results - Nacelle highlight flow angularity distortion

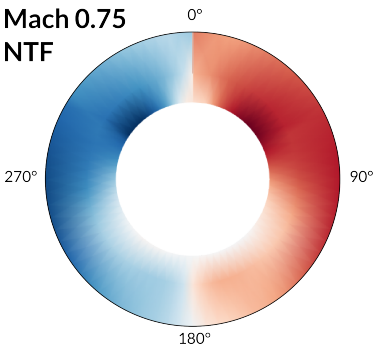
Re = 5-million, α = 2°

Mach number effects

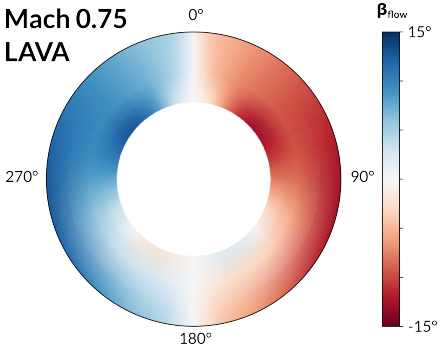
5-hole probe locations
(Credit: Chan, D., 2024)



Mach 0.75
NTF



Mach 0.75
LAVA



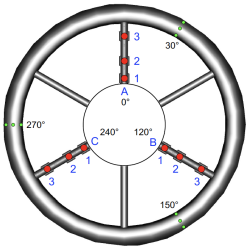
$$\beta_{\text{flow}} = \operatorname{atan} \frac{V_y}{V_x}$$

Results - Nacelle highlight flow angularity distortion

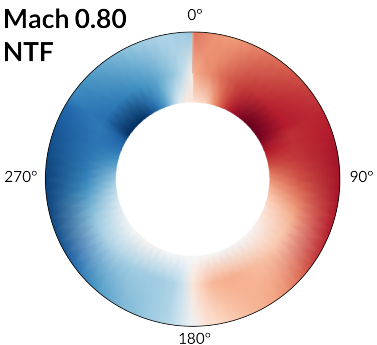
Re = 5-million, α = 2°

Mach number effects

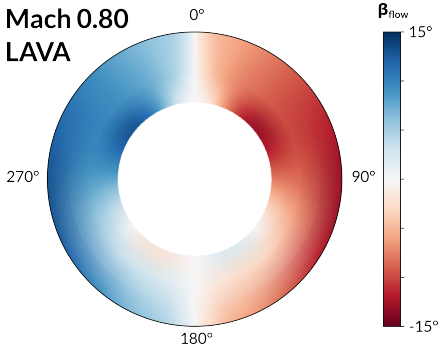
5-hole probe locations
(Credit: Chan, D., 2024)



Mach 0.80
NTF



Mach 0.80
LAVA



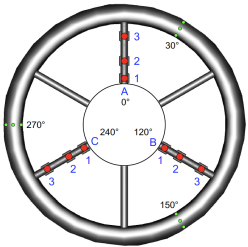
$$\beta_{\text{flow}} = \operatorname{atan} \frac{V_y}{V_x}$$

Results - Nacelle highlight flow angularity distortion

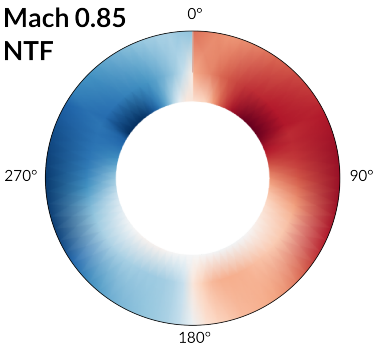
Re = 5-million, α = 2°

Mach number effects

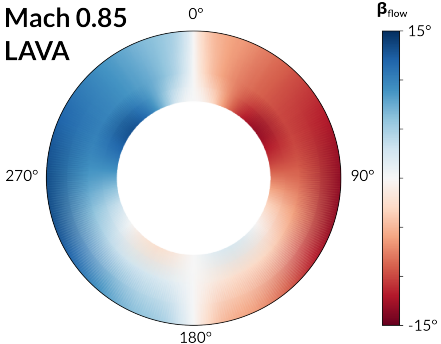
5-hole probe locations
(Credit: Chan, D., 2024)



Mach 0.85
NTF



Mach 0.85
LAVA



$$\beta_{\text{flow}} = \operatorname{atan} \frac{V_y}{V_x}$$

Summary

- Ran 205 steady RANS cases using the LAVA curvilinear solver, covering the NTF CRM-TCT test matrix conditions

Summary

- Ran 205 steady RANS cases using the LAVA curvilinear solver, covering the NTF CRM-TCT test matrix conditions
- Determined grid sizing and turbulence model closure best-practices for obtaining accurate predictions with the LAVA solver

Summary

- Ran 205 steady RANS cases using the LAVA curvilinear solver, covering the NTF CRM-TCT test matrix conditions
- Determined grid sizing and turbulence model closure best-practices for obtaining accurate predictions with the LAVA solver
- Found excellent agreement between simulations and wind tunnel data

Summary

- Ran 205 steady RANS cases using the LAVA curvilinear solver, covering the NTF CRM-TCT test matrix conditions
- Determined grid sizing and turbulence model closure best-practices for obtaining accurate predictions with the LAVA solver
- Found excellent agreement between simulations and wind tunnel data
  - Drag polar is well captured, pitching moment slightly underpredicted

Summary

- Ran 205 steady RANS cases using the LAVA curvilinear solver, covering the NTF CRM-TCT test matrix conditions
- Determined grid sizing and turbulence model closure best-practices for obtaining accurate predictions with the LAVA solver
- Found excellent agreement between simulations and wind tunnel data
  - Drag polar is well captured, pitching moment slightly underpredicted
  - Aftbody flow upstream of TCT inlet shows good agreement, except for the BL profiles at 135° and 180°

Summary

- Ran 205 steady RANS cases using the LAVA curvilinear solver, covering the NTF CRM-TCT test matrix conditions
- Determined grid sizing and turbulence model closure best-practices for obtaining accurate predictions with the LAVA solver
- Found excellent agreement between simulations and wind tunnel data
  - Drag polar is well captured, pitching moment slightly underpredicted
  - Aftbody flow upstream of TCT inlet shows good agreement, except for the BL profiles at 135° and 180°
  - Inflow distortion profiles are not adversely impacted, agree well with NTF data

Summary

- Ran 205 steady RANS cases using the LAVA curvilinear solver, covering the NTF CRM-TCT test matrix conditions
- Determined grid sizing and turbulence model closure best-practices for obtaining accurate predictions with the LAVA solver
- Found excellent agreement between simulations and wind tunnel data
  - Drag polar is well captured, pitching moment slightly underpredicted
  - Aftbody flow upstream of TCT inlet shows good agreement, except for the BL profiles at 135° and 180°
  - Inflow distortion profiles are not adversely impacted, agree well with NTF data
  - Overall trends with Reynolds number, Mach number, angle-of-attack and engine operating conditions match those observed in the tunnel

Summary

- Ran 205 steady RANS cases using the LAVA curvilinear solver, covering the NTF CRM-TCT test matrix conditions
- Determined grid sizing and turbulence model closure best-practices for obtaining accurate predictions with the LAVA solver
- Found excellent agreement between simulations and wind tunnel data
- Demonstrated that RANS-based flow analysis can be used to accurately model TCT configurations using the LAVA curvilinear flow solver

Acknowledgements

- Funding provided by NASA Aeronautics Research Mission Directorate's (ARMD) Advanced Air Transport Technology (AATT) project under Advanced Air Vehicles Program (AAVP)
- Computer resources supporting this work were provided by the NASA High-End Computing (HEC) Program through the NASA Advanced Supercomputing (NAS) facility at NASA Ames Research Center (ARC)
- Thanks to Dr. Shishir Pandya for the valuable technical guidance, Dr. Michael Bozeman for the discussions surrounding the comparisons between LAVA and the USM3D code

If you are interested in more details about this research

- **David T. Chan** et al., AIAA-2024-3515
  Experimental Investigation of a Boundary Layer Ingesting Tailcone Thruster Configuration at the National Transonic Facility

- **Luis S. Fernandes** et al., AIAA 2024-3766
  Computational Analysis of a Boundary-Layer Ingesting Tailcone Thruster Configuration Within the National Transonic Facility Using the LAVA Solver

- **Michael D. Bozeman**, AIAA 2024-4022
  USM3D-ME Analyses Performed in Support of a Wind Tunnel Test of a Boundary-Layer Ingestion Configuration